Elastic mechanism design of a CMM contact probe

Rui-Jun Li*[a, c], Kuang-Chao Fan[a, b], Hao Zhou[a], Na Wang[a], Qiang-xian Huang[a]
[a]School of Instrument Science and Opto-electric Engineering, Hefei University of Technology, Hefei , China, 230009; [b]Department of Mechanical Engineering, National Taiwan University, Taipei, Taiwan, 106; [c]Anhui Electrical Engineering Professional Technique College, Hefei, China, 230051

ABSTRACT

The measurement of miniature components with a micro- or nano-coordinate measuring machine requires a high precision contact scanning probe. The elastic mechanism of low stiffness is a major component of the contact scanning probe. A new elastic mechanism is analyzed by the theory of elasticity and finite element analysis in this paper. It is to realize the probe's mechanical behavior and stiffness when designing an elastic mechanism for a contact scanning probe. The contact scanning probe is composed of a tungsten stylus with a ruby ball tip, a mechanism of floating plate suspended by four V-shaped leaf springs, and a 3D optical sensor. The leaf spring experiences elastic deformation when a contact force is applied. Uniform stiffness model is analyzed. Simulation and experimental results verify the correctness of the analysis.

Keywords: Contact probe, elastic mechanism, Stiffness, Micro/nano-coordinate measurement machine

1. INTRODUCTION

To satisfy all kinds of demands of micro- and nano-scale dimensional metrology, a number of various probes have been developed in the last decade[1-15]. Some of them are contact scanning probes[10-15]; each main structure normally consists of an elastic mechanism and several sensors in order to detect the movement of the probe tip in all directions. The contact scanning probe must meets some rigorous requirements: (1) the contact force should be small, normally less than 1 mN, (2) the scanning repeatability should be less than 30 nm, (3) the tip ball radius should be small, normally less than 300 μm, (4) the stiffness should be low, normally less than 1 mN/μm, and symmetrical in all directions, (5) the probe have enough scanning range, at least 5 μm [10-15]. The larger the scanning range becomes, the more difficult the elastic mechanism can achieve.

The author's group previously developed a contact scanning probe whose scanning range reaches ±20 μm in all directions[15]. This paper analyzes the elastic mechanism using the theory of elasticity and finite element analysis. The uniform stiffness model is verified by the experiment.

2. THE PROBE PRINCIPLE AND STRUCTURE

The developed contact scanning probe is composed of a tungsten stylus with a ruby ball tip, an elastic mechanism of floating plate suspended by four V-shaped leaf springs, a compact 3D optical sensor based on a micro auto-collimator and a miniature Michelson linear interferometer. The structure of this 3D optical sensor is shown in Figure 1; Figure 2 shows the photo of the probe, Figure 3 shows the elastic mechanism. The stylus is inserted to the floating plate. The contact force applied to the stylus tip-ball causes the floating plate to tilt and move as a rigid body motion while the leaf springs experience elastic deformations. The tilt of the floating plate is detected by the micro auto-collimator with respect to the mirror mounted at the center of the floating plate. The vertical displacement of the plate is detected by the miniature Michelson interferometer with respect to the same mirror. With such a configuration the movement of the probe tip, due to the contact force, in X, Y and Z directions can be solved by the three sensing signals (θ, φ and Z)[15].

*liruijun001@126.com; phone +86 13856971653; fax +86 551 62903823

Sixth International Symposium on Precision Mechanical Measurements,
edited by Shenghua Ye, Yetai Fei, Proc. of SPIE Vol. 8916, 89160P
 · doi: 10.1117/12.2035794

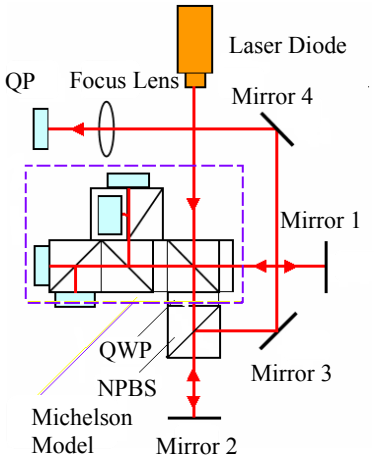

Figure 1. The structure of the 3D optical sensor

Figure 2. The photo of the probe

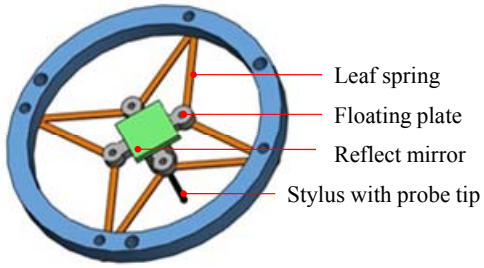

Figure 3. The structure of the elastic mechanism.

3. DESIGN ANALYSIS OF THE ELASTIC MECHANISM

The main task of the floating plate is to assure the probe a stable rest position and a tilt angle relative to the contact force in three orthogonal directions. The shape and dimension of the floating plate, as well as the length, width and thickness of the leaf springs, are determined according to the required tip ball movement and contact forces. The trigger force is normally required to be less than 1 mN and the stiffness of the probe is less than 1 mN/μm. The dimension of the mechanism can be calculated by the finite element method in order to obtain an optimum geometry. Due to its symmetrical geometry, the force-motion characterisitics will be automatically symmetrical in the X-Y plane. In order to analyze the response of the displacement to the contact force, the mechanical structure shown in Figure 4 is taken into account. Mechanical behavior under contact force can be analyzed by theory of elasticity as follows[16, 17].

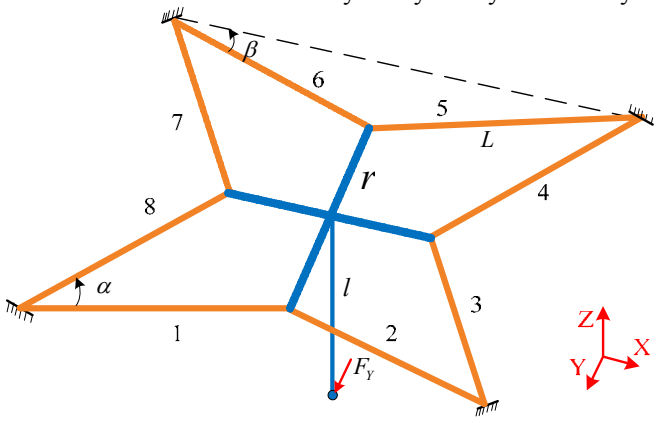

Figure 4. Simplified structure of the floating mechanism

3.1 Deformation under vertical contact force

When a vertical force (F_Z) is applied to the ball tip, all leaf springs will be deflected symmetrically in the Z-direction, as shown in Figure 5. Each leaf spring is treated as a slender thin cantilever beam, which slope at both ends should be zero, since the leaf springs are fixed on the floating plate. The free body diagrams of the floating plate and the leaf spring are shown in Figure 6. The shear force P and the bending moment M are reaction loads from the plate. Due to the geometrical symmetry of eight leaf springs, P= (F_Z/8). The bending moment in Y direction, M, is unknown and has to be found.

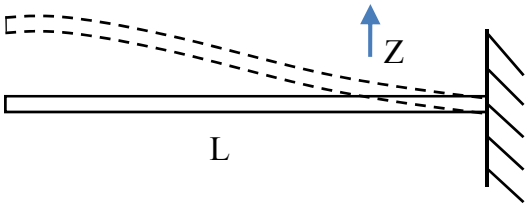

Figure 5. Deformation of each leaf spring under contact force in Z

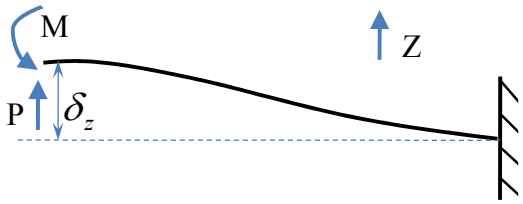

Figure 6. Free body diagrams of the leaf spring.

From the theory of elasticity, the vertical displacement and the slope at free end of leaf spring under each load can be summarized in Table 1. The torque T applied to the free end will cause a twisted angle ϕ that will be used in the next section.

Table 1: Elastic behavior at the leaf spring end under different loads

Load	Deflection	Slope
P	$\delta_1 = \frac{PL^3}{3EI}$	$\theta_1 = \frac{PL^2}{2EI}$
M	$\delta_2 = \frac{ML^2}{2EI}$	$\theta_2 = \frac{ML}{EI}$
T	---	$\phi = \frac{TL}{GJ}$

At the boundary of the leaf spring end the slope must be zero, so that $\theta_1=\theta_2$. Therefore, M can be found as

$$M = (PL)/2 \tag{1}$$

Because the floating plate is treated as a rigid body motion, the total displacement at the leaf spring end (δ_Z) is the same as the tip ball displacement.

$$\delta_{b,Z} = \delta_1 - \delta_2 \tag{2}$$

Substituting δ_1, δ_2 and M into Eq. (2), we can find the displacement of the tip ball under contact force F_z. For the case of eight suspending leaf springs, P=F_z/8, therefore, Eq. (3) is obtained. This derivation is also applicable to any N-leaf springs of suspension. A conclusion is also obtained that is: the more the suspension leaf springs the larger the probe stiffness in Z-direction.

$$\delta_{b,Z} = \frac{F_Z L^3}{96EI}$$
$$\mathrm{K}_Z = \frac{F_Z}{\delta_{b,Z}} = \frac{96EI}{L^3} \tag{3}$$

3.2 Deformation under horizontal contact force

The free body diagram of the floating plate under a contact force of Fy is shown in Figure 7, a is half the width of the arrn. Each leaf spring is treated as an elastic beam in rectangular cross section. The leaf spring is transferred a vertical

force, a torque and a bending moment from the arm at the same time, since it is not perpendicular with the arm. The vertical force on the arm will be directly reacted by the leaf spring; and the torque or bending moment on the arm will be not equal to the torque or bending moment on the leaf spring. Based on the geometrical symmetry, the loads reacted on the arm from leaf springs 1, 2, 5 and 6 are equal, and loads reacted on the arm from leaf springs 3, 4, 7 and 8 are equal. The deformed shape of leaf spring 1 and 3 can be illustrated in Figure 8. There is an angle β between the directions of the torque/bending moment and the directions of Fy/Fx. So the torque and bending moment can be decomposed into X component and the component along the Y direction. It is noted that the lateral displacement at the free end of the leaf spring is negligible as the width tothickness ratio (w/t) is larger than 10.

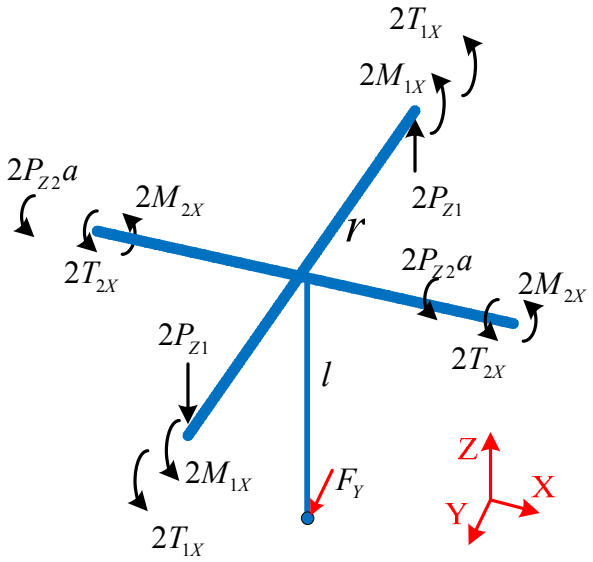

Figure 7. Free body diagram of the floating plate

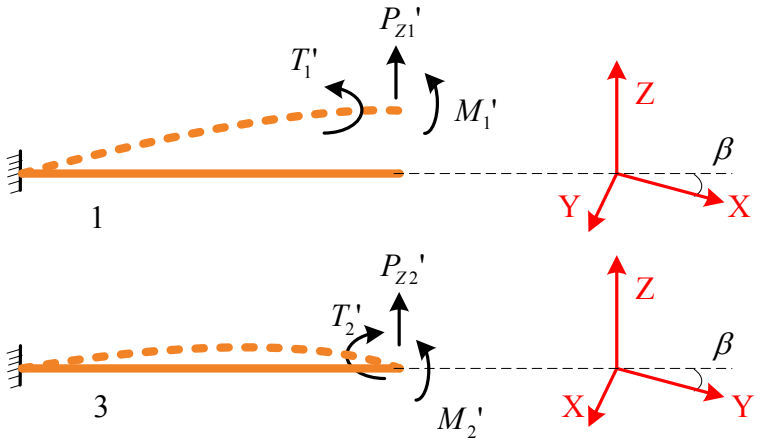

Figure 8. Deformed shape of (upper) spring 1 and (lower) spring 3

According to Figure 8, an equilibrium equation can be listed:

$$F_y l = \left(4P_{Z1}\cdot r + 4M_{1X} + 4T_{1X}\right) + \left(4P_{Z2}\cdot a + 4M_{2X} + 4T_{2X}\right) \quad (4)$$

where, $M_{1X} = M_1 \cdot \sin\beta$, $T_{1X} = T_1 \cdot \cos\beta$; $M_{2X} = M_2 \cdot \cos\beta$, $T_{2X} = T_2 \cdot \sin\beta$ (5)

Let the rotating angle of the probe be θ, the deflection, bend angle and torsion angle of the leaf spring 1 be δ_1, ς_1 and τ_1, respectively; the deflection, and the bend angle and torsion angle of the leaf spring 3 be δ_2、 ς_2 and τ_2, respectively. We can obtain[16, 17]:

$$\mathbf{P_z} = \frac{12EI\delta + 6EI\varsigma L}{L^3} \quad (6)$$

$$\mathbf{M} = \frac{6EI\delta + 4EI\varsigma L}{L^2} \quad (7)$$

$$\mathbf{T} = \frac{GJ\tau}{L} \quad (8)$$

The probe stylus is inserted into the floating plate; both are treated as a rigid body. So the floating plate's angle is:

$$\theta = \delta_{b,Y} / l$$

Since the free end of the leaf spring and the end of the arm are fixed together, the deflection of the leaf spring 1 and 3 can be expressed as:

$$\delta_1 = \delta_{b,y} \cdot r/l \quad (9)$$

$$\delta_2 = \delta_{b,y} \cdot a/l \quad (10)$$

Now, it is to find ς_1 and τ_1. From Figure 9 we can see that the plane $O_1'A_1B_1$ is the overlap between the leaf spring 1 and the arm of the floating plate. Plane $O_1'A_1B_1$ is located in the $O_1'O_1A_1B_1$ plane when the tip ball has not been touched. However, Plane $O_1'A_1B_1$ will be located in the $O_1'O_1C_1D_1$ plane when the probe has an angle θ along the Y direction (shown in Figure. 10). Because $O_1'A_1' \perp B_1A_1'$, we have $O_1'B_1 = a/\cos\beta$ and $O_1'A_1' = a \cdot \tan\beta$; and because $O_1'A_1' = O_1A_1$ and $C_1A_1 \perp A_1O_1$, so that $C_1A_1 = A_1O_1 \cdot \tan\theta = a \cdot \tan\beta \cdot \tan\theta$. Also, because $C_1A_1 = D_1B_1$ and $D_1B_1 \perp O_1'B_1$, so that $\tan\varsigma_1 = \frac{D_1B_1}{O_1'B_1} = \frac{a \cdot \tan\beta \cdot \tan\theta}{a/\cos\beta} = \sin\beta \cdot \tan\theta$, yielding $\varsigma_1 = \theta \cdot \sin\beta$. Since $O_1'A_1 = O_1'B_1 \cdot \tan\beta = \frac{a}{\cos\beta} \cdot \tan\beta$, therefore $\tan\tau_1 = \frac{C_1A_1}{O_1'A_1} = \frac{a \cdot \tan\beta \cdot \tan\theta}{a \cdot \tan\beta/\cos\beta} = \tan\theta \cdot \cos\beta$, yielding $\tau_1 = \theta \cdot \cos\beta$.

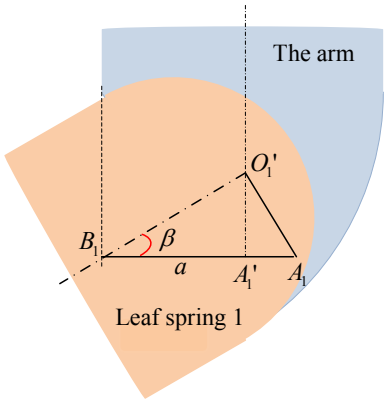

Figure 9. The overlap between the leaf spring 1 and the arm

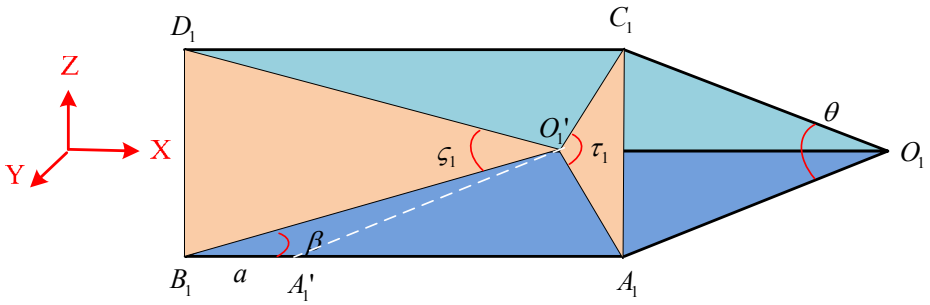

Figure 10. The deformation of the overlap between the leaf spring 1 and the arm

Similarly, plane $O_1'A_1B_1$ in Figure 11 is the overlap between the leaf spring 3 and the arm of the floating plate. Plane $O_2'A_2B_2$ is located in the $O_2'O_2A_2B_2$ plane when the tip ball has not been touched. However, Plane $O_2'A_2B_2$ will be located in the $O_2'O_2C_2D_2$ plane when the probe has an angle θ along the Y direction (shown in Figure 12). Using the same analysis, we can obtain $\varsigma_2=\theta\cdot\cos\beta$ and $\tau_2=\theta\cdot\sin\beta$ 。

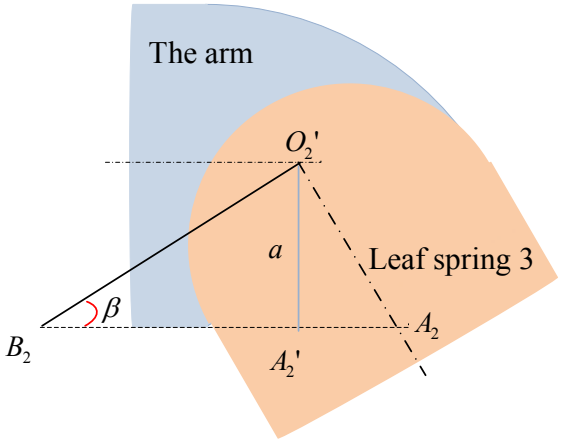

Figure 11. The overlap between the leaf spring 3 and the arm

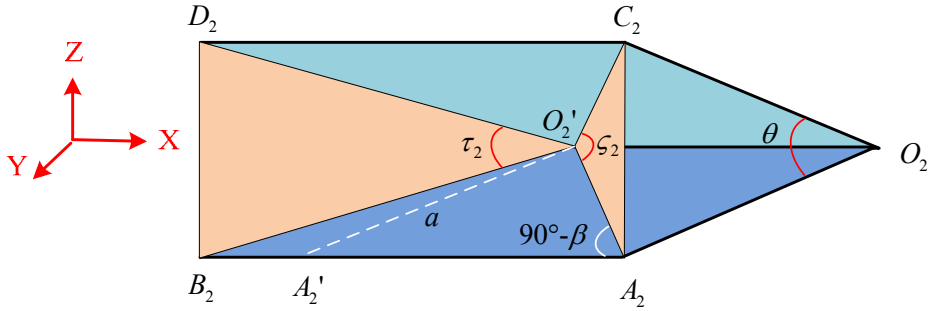

Figure 12. The deformation of the overlap between the leaf spring 3 and the arm

Substituting $\delta_1,\varsigma_1,\tau_1$ and $\delta_2,\varsigma_2,\tau_2$ into equation (6) to (8), we can obtain P_{Z1}, M_1, T_1 and P_{Z2}, M_2, T_2. Furthermore, substituting P_{Z1},M_1,T_1 and P_{Z2}, M_2, T_2 into equation (5) and (4), we can obtain the stiffness of the V shaped elastic mechanism along the Y direction.

$$K_y = F_y \Big/ \delta_{b,y} = \frac{4}{L^3 l^2}\left[GJL^2 + 2EI\left(6r^2 + 3r\sin\beta + 3rL\sin\beta + L\right) + 2EI\left(6a^2 + 3a\cos\beta + 3aL\cos\beta + L\right)\right] \quad (11)$$

where $I = \frac{wt^3}{12}$, $\mathbf{J} = \frac{wt^3}{16}\left(\frac{16}{3} - 3.36\frac{t}{w}\right)$, $G = \frac{E}{2(1+\nu)}$, ***w*** is the width of the leaf spring, ***t*** is the thickness of the leaf spring's cross section, and ***v*** is the Poisson's ratio of the leaf spring.

4. EXAMPLES

The material propoerties and the dimensions of the probe mechanism are listed in Table 2. Parameters to be used for calculation are highlighted in bold.

Table 2. The components of the probe mechanism.

Item	Specifications
Leaf springs	Material: Beryllium-copper alloy, **E=130×10^9 Pa, thickness:0.1 mm, width: 2 mm, length: *L*=13 mm**
Floating plate	Material: aluminum alloy, $E = 7.1\times10^{10}\,Pa$, thickness:1.5 mm, **arm length: *r*=5.5 mm**, arm width:2 mm; weight:1.3 g
Stylus	Material: tungsten stylus with a ruby ball tip , $E = 1.93\times10^{11}\,Pa$, length: ***l*=10 mm**, diameter 0.5 mm

4.1 Analytical results

The stiffness in Z direction $K_z(F_z/\delta_{b,z})$ is obtained as 0.943 N/mm. In order to find uniform stiffness in all directions, the stylus length (*l*) is the most convenient one to be adjusted. Let equation (3) be equal to equation (11), the value of *l* can be obtained as 9.6 mm. Then, K_y will be the same as K_z (0.943 N/mm).

4.2 Simulation results

In order to validate the correctness of the stiffness model, computer simulation is also carried out using ANSYS V12 (finite element analysis software). The parameters shown in Table 2 are taken in use. The tip's displacement is shown in Figure 13 (a) and 13 (b) when it is applied a 1 mN force in horizontal and in vertical direction respectively, the tip move both 0.926 μm, The analytical results are coincided with the simulated results quite well and the differences are less than 1.8%. Figure 13 (c) is the result when it is applied a 1 mN force in different directions. We can see that the elastic mechanism is quite uniform.

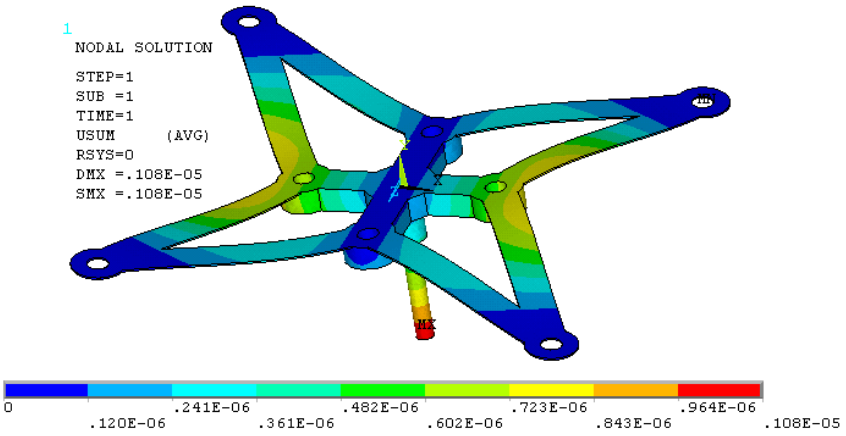

(a) Contacting with a 1 mN force in horizontal

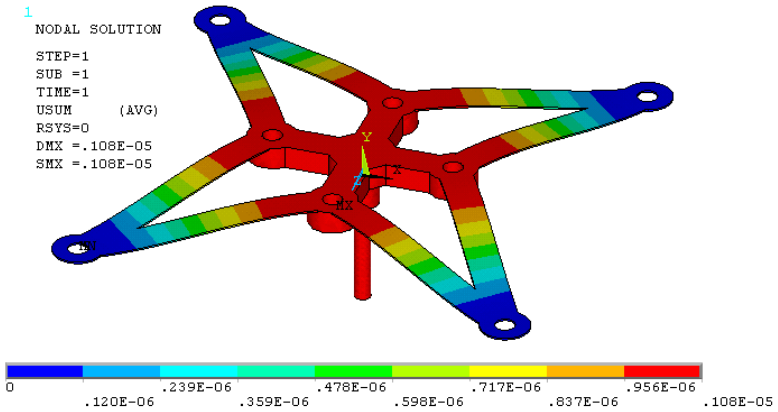

(b) Contacting with a 1 mN force in vertical

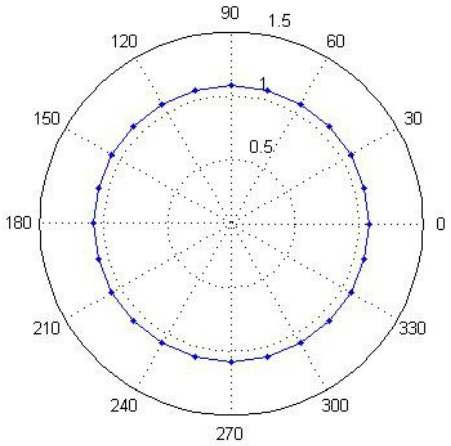

(c) Contacting with a 1 mN force in different directions

Figure 13. the tip's displacement when contacting force is applied

4.3 Experimental results

A very sensitive force measurement apparatus also has been designed, as shown in Figure 14. A thin copper plate is built in to the base. When a small force is applied to its end, a bending angle can be detected by an angular sensor, which is made from a miniature angular Michelson interferometer whose two beams are reflected by the same mirror. This force sensor has been calibrated by some known weights with very good linearity. In this experiment, the force sensor was carried by a linear stage, which displacement was measured by a capacitance sensor. Figure 15 shows the photo of experimental setup. The experimental results show the stiffness in Z direction was 0.954 N/mm and in the horizontal plane was 0.927 N/mm in average, being quite close to the analytical and simulation results. The difference of less than 1.7% could be due to the manufacture and assembly errors of the probe.

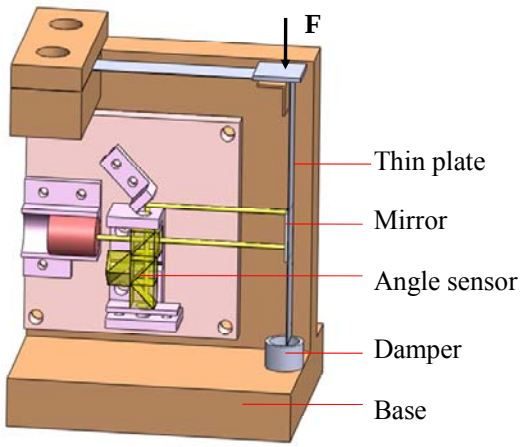

Figure 14. The photo of the measuring contact force

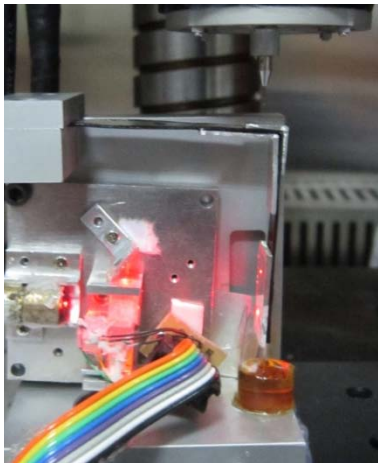

Figure 15. Photo of experimental setup

5. CONCLUSIONS

This paper analyzes the elastic mechanism of a contact scanning probe for a micro-CMM. The innovative probe consists of a probe stylus; a mechanical floating mechanism with four V-shape leaf springs suspension, and a 3D optical sensor. The deformation analysis of the elastic mechanism has been carried out using the elasticity theory. Its uniform stiffness model is analyzed. Simulation and experimental results verify the correctness of the analysis. From the uniform stiffness model, it is effective to design a probe mechanism of this cross-shape floating plate suspended by four V-shape leaf springs with constant stiffness in all directions.

ACKNOWLEDGMENT

The work reported is part of a research program funded by the National Natural Science Foundation of China (Grant Nos. 50875073 and 51275148), the National High Technology Research and Development Program (863) of China (Grant No. 2008AA042409).

REFERENCES

[1] K. C. Fan, Y. T. Fei, X. F. Yu, et al., "Development of a Low-Cost Micro-CMM for 3D Micro- and Nanomeasurements,"Meas. Sci. Technol. 17 (3), 524–532 (2006).
[2] G. Jäger, E. Manske, and T. Hausotte, "Nanopositioning and Measuring Machine," in Proc. of the 2nd EUSPEN Int. Conf., 1, 290–293(2001).
[3] K. Takamasu, K. R. Furutani, and S. Ozono, "Development of Nano-CMM (Coordinate Measuring Machine with Nanometer Resolution)," in Proc. of the XIV IMEKO World Congress, 8, 34–39(1997).
[4] G. N. Peggs, A. J. Lewis, and S. Oldfield, "Design for a Compact High-Accuracy CMM," Ann. CIRP. 48 (1), 417–420 (1999).
[5] H. Haitjema, W. O. Pril, and P. Schellekens, "Development of a Silicon-Based Nanoprobe System for 3-D Measurements," Ann. CIRP 50 (1), 365–368 (2001).
[6] H. Ji, H. Y. Hsu, L. X. Kong, and A. B. Wedding, "Development of a Contact Probe Incorporating a Bragg Grating Strain Sensor for Nano Coordinate Measuring Machines," Meas. Sci. Technol. 20 (9), 095304 (2009).
[7] Gyula Hermann, Csongor Sántha "Design of Tactile Measuring Probes for Coordinate Measuring Machines" Acta Polytechnica Hungarica , 6, 1 (2009)
[8] C. L. Chu and C. Y. Chiu, "Development of a Low Cost Nanoscale Touch Trigger Probe Based on Two Commercial DVD Pick-up Heads," Meas. Sci. Technol. 18 (7), 1831–1842 (2007).
[9] A. Weckenmann, G. Peggs, and J. Hoffmann, "Probing Systems for Dimensional Micro- and Nano-Metrology,"Meas. Sci. Technol. 17 (3), 504–509 (2006).
[10] Leach, R K, Murphy, J "The design of co-ordinate measuring probe for characterising truly three-dimensional micro-structures". 4th euspen International Conference, Glasgow, UK, 31, 230-231 (2004).

[11] F. Meili, M. Fracheboud, S. Bottinelli, etc. “High precison , Low force 3D touch probe for measurements on small objects”, European Int. Topical Conf., Achend, Germany, Extended abstract(2003).
[12] A. Küng, F. Meli, and R. Thalmann, “Ultraprecision Micro-CMM Using a Low Force 3D Touch Probe,” Meas. Sci. Technol. 18 (2), 319–327 (2007).
[13] K. C. Fan, F. Cheng, W. L.Wang, et al., “A Scanning Contact Probe for a Micro Coordinate Measuring Machines (CMM),” Meas. Sci. Technol. 21 (5), 054002 (2010).
[14] Balzer, F.G., Hausotte, T., Dorozhovets, N., Manske, E., Jager, G., “Tactile 3D microprobe system with exchangeable styli” Meas. Sci. Technol., 22, 9 (2011).
[15] Rui-Jun Li, Kuang-Chao Fan, Qiang-Xian. Huang, etc. “Design of a Large Scanning Range Contact Probe for Nano-Coordinate Measurement Machines (CMM),” Optical Engineering, 51, 8, 081503 (2012).
[16] K.C. Fan, F. Cheng, W.T. Pan, etc., “Analysis of a contact probe mechanism for micro-coordinate measuring machines,” Optoelectronics, Instrumentation and Data Processing, 46, 4, 340-346 (2010).
[17] R. J. Li, S. Tao, K.C. Fan, etc, “Analysis of an elastic mechanism for contact scanning probe,” Proc. of SPIE, 8769, 87590M (2012).